energies

MDPI

Article

Grid Current Feedback Active Damping Control Based on Disturbance Observer for Battery Energy Storage Power Conversion System with LCL Filter

Ning Gao [1,*], Xin Lin [1], Weimin Wu [1,*] and Frede Blaabjerg [2]

[1] Department of Electrical Engineering, Shanghai Maritime University, Shanghai 201306, China; 201930210084@stu.shmtu.edu.cn
[2] Department of Energy Technology, Aalborg University, DK-9220 Aalborg, Denmark; fbl@et.aau.dk
* Correspondence: ngao@shmtu.edu.cn (N.G.); wmwu@shmtu.edu.cn (W.W.)

Abstract: Adopting the battery energy storage system is an effective way to compensate the continuously growing fluctuating power generated by renewable sources. The power conversion system is considered as one of the core equipment used for interfacing battery packs to the grid in a battery energy storage system. This paper aims to apply an improved active damping control to a grid-tied power conversion system with LCL filter to attenuate its inherent resonance characteristics. The anti-interference ability is enhanced by estimating the second-order derivation of grid-injected current based on a modified disturbance observer. Meanwhile, the negative effects of parameter mismatch are equivalent to unmeasurable disturbances, which are possible to be compensated by subtracting the estimated values from the modulated voltage references. Moreover, the design method and robustness issue of the disturbance observer are discussed in detail. The presented control algorithm is implemented based on Simulink and dSpace. Detailed simulation results are provided, which can verify the feasibility and correctness of control strategy. Furthermore, an experimental prototype rated at 2.3 kW/110 V is constructed. The experimental results confirm that the presented control method is effective to be applied in the power conversion system (PCS).

Keywords: battery energy storage system; power conversion system; LCL filter; active damping; disturbance observer

check for updates

Citation: Gao, N.; Lin, X.; Wu, W.; Blaabjerg, F. Grid Current Feedback Active Damping Control Based on Disturbance Observer for Battery Energy Storage Power Conversion System with LCL Filter. *Energies* **2021**, *14*, 1482. https://doi.org/10.3390/en14051482

Academic Editor: Antonino Laudani

Received: 5 February 2021
Accepted: 1 March 2021
Published: 8 March 2021

Publisher's Note: MDPI stays neutral with regard to jurisdictional claims in published maps and institutional affiliations.

Copyright: © 2021 by the authors. Licensee MDPI, Basel, Switzerland. This article is an open access article distributed under the terms and conditions of the Creative Commons Attribution (CC BY) license (https://creativecommons.org/licenses/by/4.0/).

1. Introduction

The everlasting development of renewable generation systems brings about a potential challenge to the stability of grid, since the balance between electrical energy providers and consumers recently becomes much harder to be maintained [1,2]. In such a context, energy storage technology is believed to be one of the best choices to solve this problem [3]. Battery energy storage system (BESS), characterized by its high energy density, high efficiency, flexibility and fast response, is highly suitable to perform as an energy buffer in renewable generation applications [3,4]. As a result, the research about BESS is rapidly gaining more and more attentions in recent years.

Power conversion system (PCS), which can be classified to a dedicated kind of grid-tied converter, is the intermediate power electronics equipment between battery packs and grid. Its main task is to transfer the electrical energy stored in the battery packs bi-directionally to the grid through semiconductor switches and a passive low-pass filter [5,6]. Benefit from its lower cost and better high frequency suppression performance, PCS usually contains an LCL filter to attenuate the high frequency ripples generated by the switching process of power devices. However, the inherent resonance feature also leads to stability issue in evidence. To deal with this problem, additional damping method needs to be adopted and a lot of related researches have been done so far for decades.

Passive damping is the simplest way to stabilize LCL filter by adding extra resistors in the circuit. Although this scheme is effective and easy to implement, additional power loss

and increased cost restrict its further applications [7–9]. By properly changing the circuit structure, a series of modified high-order filter, such as LLCL filter, can be obtained. It is believed that the frequency domain feature of these filter topology is improved but the resonance peak is still difficult to be totally eliminated [10,11]. Therefore, active damping (AD) techniques are taken into account by feeding back specified variables (single variable or combination of variables) inside the filter or embedding an internal digital filter into the controller to modify the forward path [12]. Because AD only needs to change the control loop in the processor without introducing additional components, it becomes more preferable than passive damping techniques now.

L. Zhou et.al combined a first-order high-pass filter with converter-side current feedback loop in [13] for distributed generation system. The analysis in [13] shows that this is equivalent to create a virtual impedance connected with the converter-side inductor in series, which is helpful to suppress the original resonance peak with a reduced frequency offset. Literature [14] proposed a novel AD algorithm based on negative resonance regulator and grid-current feedback. The outstanding advantages of this algorithm includes lower switching noise sensitivity and superior control delay compensation. The performance of inverter was also tested while connecting to a weak grid. Ref. [15] embedded a digital notch filter implemented based on direct-form II transposed in the controller to tackle the resonance issue caused by the uncertain parameter drift of main circuits. It is found that this AD strategy tolerates the resonance frequency drifting well by sufficient experimental verifications. In [16], a hybrid AD algorithm based on capacitor current feedback and point of common coupling voltage feedback was proposed. The cooperation between these two individual feedback channels can provide the maximum profit to ensure the robustness of AD in cases parameter variation and non-ideal grid takes place. Similar damping requirement is also significant for stand-alone inverter applications. The authors in [17] employed a selective frequency scheme which localized the influence scope of AD loop only near the resonance frequency; thus, the inverter's feature in other frequency range stayed the same to provide better steady and dynamic performances.

For another aspect, disturbances and uncertainties are inevitable in most practical industrial applications. These unfavorable factors usually cause performance degradation. To combat this issue, disturbance/uncertainty estimation and attenuation has become a long-lasting topic both in academia and industry since early 1960s [18]. This technique is a powerful tool for optimizing the trade-off process between disturbance rejection and rapidity, steady-state performance and robustness of the closed-loop controlled object. Within the related engineering fields, a lot of implementing approaches have been proposed.

Literature [19] designed and implemented a novel controller combined with traditional feedback loops and disturbance observer (DOB) based control. The key advantage of this controller is that it can maintain the original fast dynamic response achieved by feedback control even in the presence of external perturbation and model mismatch. Literature [20] proposed a control strategy based on active disturbance rejection control by selecting grid-side current as the unique feedback signal. The inverter possesses stronger robustness against parameter fluctuation after the adoption of extended state observer which can mathematically transforms the inverter downgrade to a simple gain module. Similarly, Ref. [21] proposed a simplification method to achieve order reduction for the plant transfer function of LCL filter by utilizing Pade approximation and extended state observer. Furthermore, DOB has been integrated with other control methods such as finite set model predictive control [22]. In [23], DOB was also applied to a grid-tied converter based on five-level T-type AC-DC topology to improve its disturbance rejection capability towards dc-bus load variation. Stability improvement of DC-DC converter can also be achieved by properly introducing DOB [24]. These cases prove that DOB is widely applicable. Therefore, an AD control strategy based on DOB for PCS is presented as an enhancement of stability and robustness in this paper.

The subsequent part of this paper is organized as following: Section 2 describes the basic principle of AD for LCL filter and implementation of DOB. Section 3 discusses the

parametric design and stability issue of the observer. Section 4 establishes the simulation model in the environment of Matlab/Simulink. Simulation results are provided in this section. Prototype is constructed and Section 4 also introduces the experimental results. Finally, Section 5 concludes the paper.

2. Principle of Active Damping Control and Disturbance Observer

Figure 1 briefly illustrates the block diagram and control principle of PCS on basis of a widely-used two-level voltage source converter. The DC terminals of PCS are connected to the battery packs which perform as the main static energy storage components in the BESS. Within a relatively short time scale, the output voltage of battery packs, denoted as U_{dc}, can be assumed to be constant. Meanwhile the AC terminals of PCS are connected to a standard three-phase three-wire grid. With sinusoidal pulse width modulation technology and grid voltage-oriented vector control, the PCS is capable of transferring AC energy from the grid to dc energy stored in the battery packs and vice versa in order to manage charging or discharging power flexibly and quickly according to the upstream grid instructions. LCL filter is used to attenuate the high order harmonic generated by the PCS.

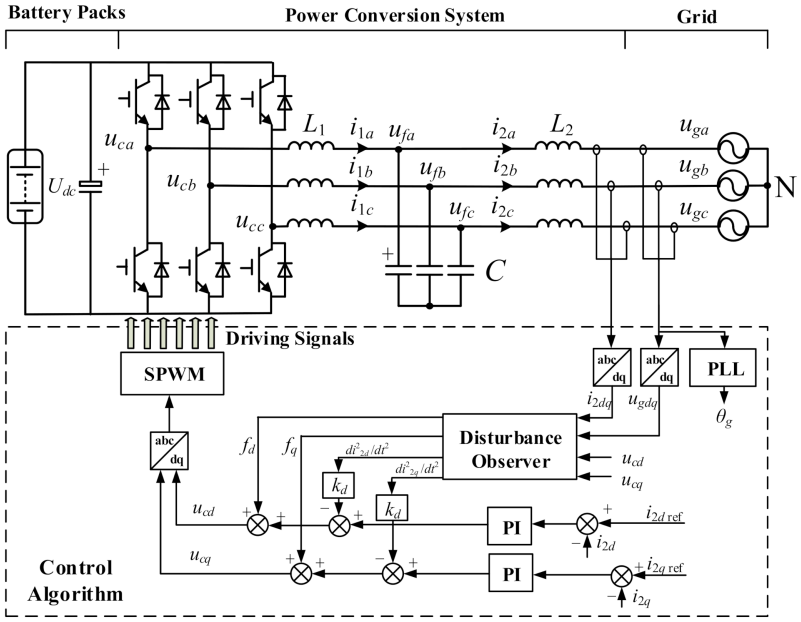


Figure 1. Basic block diagram and control principle of battery energy storage PCS.

For ease of description, In Figure 1, L_1 represents the converter-side inductor, C is the filter capacitor, L_2 represents the grid-side inductor, these passive components formed a three-order LCL filter together. The parasitic resistances of L_1 and L_2 are defined as R_1 and R_2 respectively. The output voltages per phase leg are denoted as u_{ca}, u_{cb} and u_{cc}. Converter-side currents are denoted as i_{1a}, i_{2b} and i_{2c}. Grid-side currents are represented by i_{2a} i_{2b} and i_{2c}. Instantaneous voltages of filter capacitors are u_{fa}, u_{fb} and u_{fc}. Three-phase grid voltage are represented by u_{ga}, u_{gb} and u_{gc}. The subscripts a–c represent the phase sequence respectively. The grid-side power is the ultimate control target of PCS. By adjusting i_{2d} and i_{2q}, active power and reactive power can be adjusted separately.

By applying dq-transformation, the grid-tied PCS can be modelled and separated into two subsystem, d-axis and q axis subsystems, in the synchronous rotating frame. The angle for dq-transform is calculated according to grid voltage by a phase locked loop (PLL). The coupling term between these two subsystems can be regarded as the internal disturbance and assumed to be ignorable at first, the block diagram of control loop for d-axis subsystem is given in Figure 2.

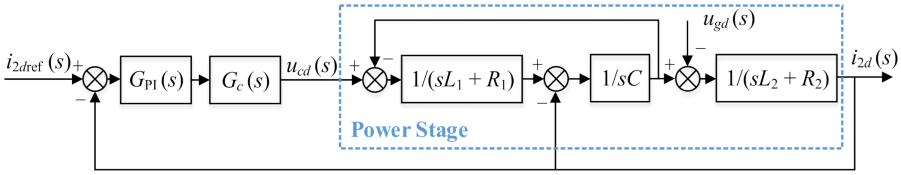


Figure 2. Block diagram of control loop for d-axis subsystem.

Meanwhile, the q-axis subsystem has the identical structure as Figure 2. Therefore, only d-axis subsystem is necessary to be discussed. Proportional integral (PI) regulator is usually selected to be inserted in the forward path in order to handle the closed-loop control of i_{2d} and i_{2q}. The transfer function of G_{PI} (s) equals to

$$G_{PI}(s) = k_p + \frac{k_i}{s} \tag{1}$$

where k_p and k_i are the proportional and integral coefficient of PI controller. G_c (s) represents the model of the voltage source converter, which can be approximated to the form of Equation (2) by neglecting modulation and sampling delay, where K_{PWM} is the modulation coefficient and U_{tri} is the carrier amplitude in SPWM module.

$$G_c(s) = K_{PWM} = \frac{U_{dc}}{U_{tri}} \tag{2}$$

Then, the original frequency domain characteristics of LCL filter can be described by Equation (3)

$$\begin{aligned} \frac{i_{2d}(s)}{u_{cd}(s)} &= \frac{1}{L_1L_2Cs^3+(R_1L_2+R_2L_1)Cs^2+(R_1R_2C+L_1+L_2)s+(R_1+R_2)} \\ &\approx \frac{1}{L_1L_2Cs^3+(L_1+L_2)s+(R_1+R_2)} \end{aligned} \tag{3}$$

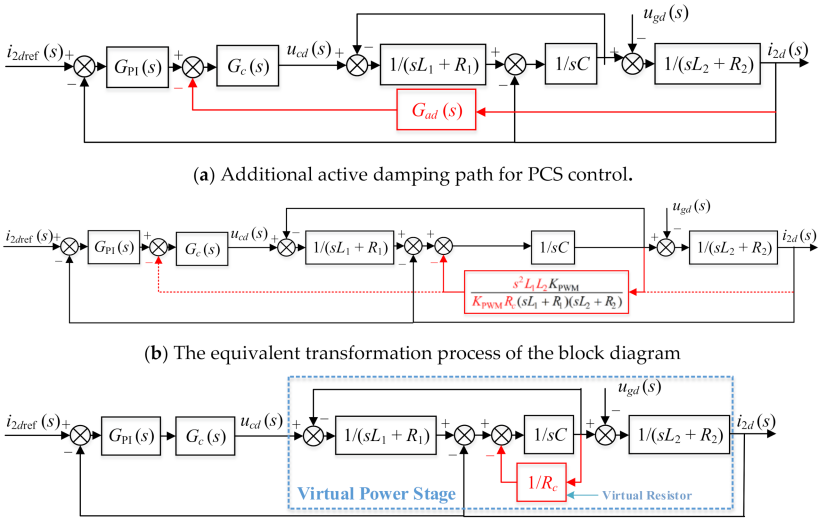
Usually, the parasitic resistance is very small in practice and can be ignored. Obliviously, there are three poles in the system. One pole locates at the origin point of complex plane and the other two poles locate conjugatively on the imaginary axis, which means the system tends to oscillate with the resonance frequency f_r depicted in Equation (4). This is not acceptable for most industrial applications.

$$f_r = \frac{1}{2\pi}\sqrt{\frac{L_1+L_2}{L_1L_2C}} \tag{4}$$

Therefore, it is necessary to adopt either active or passive damping methods to attenuate the resonance peak of LCL filter for purpose of guaranteeing the stability of PCS. AD method is usually preferable since it avoids additional power loss and passive components. To achieve AD, it is possible to reconfigure the control loop by adding a feedback branch from i_2 to u_c. The equivalent transfer function of PCS's power stage can be changed to the desired form after properly setting $G_{ad}(s)$ as

$$G_{ad}(s) = \frac{(sL_1+R_1)(sL_2+R_2)}{K_{PWM}R_c} \approx \frac{s^2L_1L_2}{K_{PWM}R_c} \tag{5}$$

After involving the additional AD path, the equivalent block diagram can be simplified from Figure 3a–c. According to the modified block diagram, it can be found that adding $G_{ad}(s)$ in the control loop has the same effect as connecting a virtual resistor R_c in parallel with filter capacitor which can be described by Figure 4. The LCL circuit is converted to an LCRL circuit.



(**a**) Additional active damping path for PCS control.

(**b**) The equivalent transformation process of the block diagram

(**c**) Equivalent block diagram for the damped virtual power stage

Figure 3. Block diagram for active damping method by applying virtual resistor in parallel with the filter capacitor.

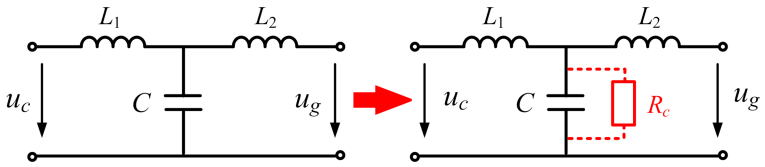


Figure 4. Equivalent circuit of LCL filter after adopting active damping.

The value of virtual resistor equals to the control parameter R_c. Therefore, it is much easier to be adjusted compare to traditional passive damping method. The corresponding bode diagram is shown in Figure 5 as a comparison for different R_c values. It can be seen according to Figure 5 that the resonance of the LCL filter is effectively suppressed after adding the above feedback branch for AD. In addition, when the damping resistance increases, the resonance suppression effect will be weakened.

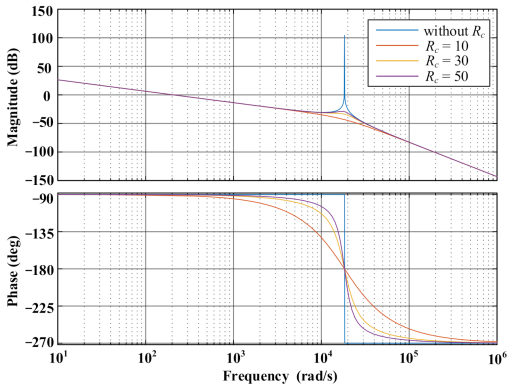


Figure 5. Bode diagram of LCL filter with different virtual damping resistors R_c.

However, the anti-interference ability of PCS tends to be poor due to the adoption of the second-order derivation of grid-injected current. The noise of sampling circuit and current sensors both become potential threats to the stability and accuracy of control method. The direct calculation of d^2i_{2d}/dt^2 and d^2i_{2q}/dt^2 and is difficult to be achieved and this is assumed to be the main drawback of AD method depicted in Figure 3a. On the other hand, the output voltage is not accurate due to the non-ideal features of power switches

and inevitable dead band. Moreover, the firstly omitted coupling effect between d-axis and q-axis subsystems can also be regarded as an unknown disturbance. In order to solve these problems, this paper presents a DOB to estimate d^2i_{2d}/dt^2 and d^2i_{2q}/dt^2 together with the unmeasurable disturbances denoted as f_d and f_q. Based on the observer, the disturbances are possible to be compensated by subtracting f_d and f_q from the reference voltages u_d and u_q, respectively. According to Figure 2, Equation (6) can be derived as

$$\begin{cases} L_1L_2C\frac{d^3i_{2d}}{dt^3} + (R_1L_2 + R_2L_1)C\frac{d^2i_{2d}}{dt^2} + (R_1R_2C + L_1 + L_2)\frac{di_{2d}}{dt} + (R_1 + R_2)i_{2d} = u_{cd} - L_1C\frac{d^2u_{gd}}{dt^2} - R_1C\frac{du_{gd}}{dt} - u_{gd} \\ L_1L_2C\frac{d^3i_{2q}}{dt^3} + (R_1L_2 + R_2L_1)C\frac{d^2i_{2q}}{dt^2} + (R_1R_2C + L_1 + L_2)\frac{di_{2q}}{dt} + (R_1 + R_2)i_{2q} = u_{cq} - L_1C\frac{d^2u_{gq}}{dt^2} - R_1C\frac{du_{gq}}{dt} - u_{gq} \end{cases} \tag{6}$$

The first and second order differential terms of the grid voltage in Equation (6) can also be included in the disturbance quantity, the right-side of Equation (6) represents the control variables which contains unknown disturbances. By rewriting Equation (6) in the form of differential equations set, we can obtain Equation (7).

$$\begin{cases} \frac{d^3i_{2d}}{dt^3} + \left(\frac{R_1}{L_1} + \frac{R_2}{L_2}\right)\frac{d^2i_{2d}}{dt^2} + \frac{R_1R_2C+L_1+L_2}{L_1L_2C}\cdot\frac{di_{2d}}{dt} + \frac{R_1+R_2}{L_1L_2C}i_{2d} + \frac{1}{L_1L_2C}f_d = \frac{1}{L_1L_2C}(u_{cd} - u_{gd}) \\ \frac{d^3i_{2q}}{dt^3} + \left(\frac{R_1}{L_1} + \frac{R_2}{L_2}\right)\frac{d^2i_{2q}}{dt^2} + \frac{R_1R_2C+L_1+L_2}{L_1L_2C}\cdot\frac{di_{2q}}{dt} + \frac{R_1+R_2}{L_1L_2C}i_{2q} + \frac{1}{L_1L_2C}f_q = \frac{1}{L_1L_2C}(u_{cq} - u_{gq}) \end{cases} \tag{7}$$

To simplify the expression, let

$$h_1 = \frac{R_1 + R_2}{L_1L_2C}, h_2 = \frac{R_1R_2C + L_1 + L_2}{L_1L_2C}, h_3 = \frac{R_1}{L_1} + \frac{R_2}{L_2}, h_4 = \frac{1}{L_1L_2C} \tag{8}$$

According to Equation (7), we can properly select the state space $x = [x_1\ x_2\ x_3\ x_4\ x_5\ x_6\ x_7\ x_8]^\mathrm{T}$, which is further defined in Equation (9) to construct the mathematical model of PCS.

$$\begin{aligned} &x_1 = i_{2d}, x_2 = \frac{di_{2d}}{dt}, x_3 = \frac{d^2i_{2d}}{dt^2}, x_4 = i_{2q}, \\ &x_5 = \frac{di_{2q}}{dt}, x_6 = \frac{d^2i_{2q}}{dt^2}, x_7 = f_d, x_8 = f_q \end{aligned} \tag{9}$$

These state variables can be regarded as constants in steady state in the dq reference frame. On the basis of this assumption, state space model can be further derived as

$$\begin{cases} \dot{x}_1 = x_2 \\ \dot{x}_2 = x_3 \\ \dot{x}_3 = -h_1x_1 - h_2x_2 - h_3x_3 - h_4x_7 + h_4(u_{cd} - u_{gd}) \\ \dot{x}_4 = x_5 \\ \dot{x}_5 = x_6 \\ \dot{x}_6 = -h_1x_4 - h_2x_5 - h_3x_6 - h_4x_8 + h_4(u_{cq} - u_{gq}) \\ \dot{x}_7 = 0 \\ \dot{x}_8 = 0 \end{cases} \tag{10}$$

Rewrite Equation (10) into the standard matrix form

$$\begin{cases} \frac{dx}{dt} = Ax + Bu \\ y = C_0x \end{cases} \tag{11}$$

where

$$\begin{aligned} u = \begin{bmatrix} u_{cd} - u_{gd} & u_{cq} - u_{gq} \end{bmatrix}^T, y = \begin{bmatrix} i_{2d} & i_{2q} \end{bmatrix}^T \\ A = \begin{bmatrix} a & 0_{3\times3} & -b_1 \\ 0_{3\times3} & a & -b_2 \\ 0_{2\times3} & 0_{2\times3} & 0_{2\times2} \end{bmatrix}, a = \begin{bmatrix} 0 & 1 & 0 \\ 0 & 0 & 1 \\ -h_1 & -h_2 & -h_3 \end{bmatrix} \\ B = \begin{bmatrix} b_1 \\ b_2 \\ 0_{2\times2} \end{bmatrix}, b_1 = \begin{bmatrix} 0 & 0 \\ 0 & 0 \\ h_4 & 0 \end{bmatrix}, b_2 = \begin{bmatrix} 0 & 0 \\ 0 & 0 \\ 0 & h_4 \end{bmatrix}, C_0 = \begin{bmatrix} 1 & 0_{1\times2} & 0 & 0_{1\times4} \\ 0 & 0_{1\times2} & 1 & 0_{1\times4} \end{bmatrix} \end{aligned} \tag{12}$$

The observability of system should be checked first. Thus, the rank of observability judgment matrix N is calculated.

$$\mathrm{Rank}(N) = \mathrm{Rank}[\ {C_0}^T \quad A^T{C_0}^T \quad (A^2)^T{C_0}^T \quad (A^3)^T{C_0}^T \quad (A^4)^T{C_0}^T \quad (A^5)^T{C_0}^T \quad (A^6)^T{C_0}^T \quad (A^7)^T{C_0}^T\ ] = 8 \tag{13}$$

According to the calculation result in Equation (13), it can be found that N is full ranked. Therefore, it is feasible to construct an observer to estimate d^2i_{2d}/dt^2, d^2i_{2q}/dt^2, f_d and f_q. Full state observer and dimensionality reduction observer are both good choices for state estimation. In this paper, full state observer is selected because of its better stability performance. The DOB is established in Equation (14)

$$\begin{cases} \frac{d\hat{x}}{dt} = A\hat{x} + Bu + M(y - \hat{y}) = (A - MC_0)\hat{x} + Bu + My \\ \hat{y} = C_0\hat{x} \end{cases} \tag{14}$$

where $\hat{x}$ represents the estimated value of x. The feedback matrix M performs a correction function to the DOB, it can be expressed as

$$M = \begin{bmatrix} g_1 & g_1 & g_1 & 0 & 0 & 0 & g_2 & 0 \\ 0 & 0 & 0 & g_1 & g_1 & g_1 & 0 & g_2 \end{bmatrix}^T \tag{15}$$

where g_1, g_2 are parameters to be determined, which decide the pole distribution and the stability of observer. Then, Equation (14) is discretized to Equation (16) based on explicit Euler method. Define T_s as the sampling period,

$$\begin{cases} \hat{x}(k+1) = (G - M_dC_0)\hat{x}(k) + Hu(k) + M_dy(k) \\ \hat{y}(k) = C_0\hat{x}(k) \end{cases} \tag{16}$$

where

$$G = e^{AT_s}, H = \int_0^{T_s} e^{A\tau}d\tau B, M_d = \int_0^{T_s} e^{A\tau}d\tau M \tag{17}$$

Finally, as a summary, the signal flow diagram of DOB is shown in Figure 6, which aims to depict the relationship between the actual and observed value of PCS. The observer takes the difference between the converter output voltage and the grid voltage as the input and uses the error between actual grid-side current and the observed current as the feedback correction, so that the observer state variables are possible to converge to the realistic system variables. Then, the observed values of disturbances and second-order differential of grid-side current are obtained. Moreover, in the next section, stability analysis and design of Matrix M will be discussed in detail.

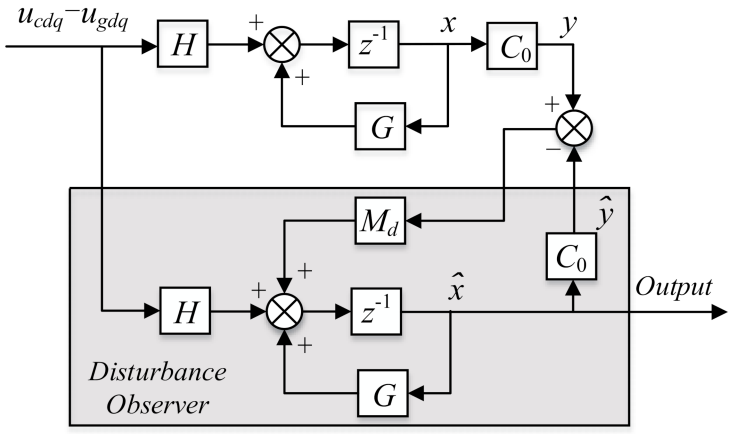


Figure 6. Structure illustration of the proposed disturbance observer.

3. Stability Analysis and Parametric Design of the Disturbance Observer

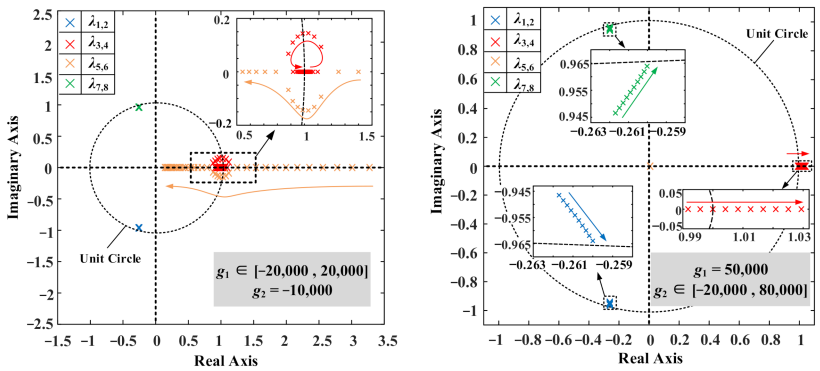
The performance and stability of DOB highly rely on the parametric design of feedback matrix. If the initial estimation error of x is defined as $\Delta x(0)$, after k periods iteration, the final observing error $\Delta x(k)$ can be expressed as

$$\Delta x(k) = (G - M_d C_0)^k \Delta x(0) \tag{18}$$

Therefore, it can be deduced that the stability and convergence of DOB is determined by the eigenvalue of $G-M_dC_0$. For theoretical analysis afterwards, the parameters of main circuit can be referred to Table 1 in Section 3. Figure 7 shows the locus of the eigenvalue distribution of the matrix $G-M_dC_0$ when M_d changes. It is worth nothing that the observer presented in this paper has a simplified process of ignoring the internal coupling term of the d and q axis when modeling, so it can be considered that the d axis and q axis are dependent with each other and have a completely symmetric characteristic eigenvalue distribution.

Table 1. Main circuit and control parameters for the PCS.

Symbols	Parameters	Value/Unit
P_n	Rated power of PCS	2.3 kW
u_g	Phase voltage of grid (RMS)	110 V_{rms}
f_g	Nominal grid frequency	50 Hz
U_{dc}	Nominal voltage of battery packs	350 V_{dc}
L_1	Converter-side inductor	3.6 mH
L_2	Grid-side inductor	1.2 mH
C	Filter capacitor	3.3 μF
R_1	Parasitic resistance of L_1	0.1 Ω
R_2	Parasitic resistance of L_2	0.05 Ω
k_d	Differential feedback coefficient	8.64×10^{-8}
k_p	Coefficients for PI controller	2
k_i		400
g_1	Coefficients for feedback loop of DOB	50,000
g_2		−12,800
f_s	Sampling & Switching frequency	10 kHz



(**a**) Pole distribution when g_1 changes (**b**) Pole distribution when g_2 changes

Figure 7. Pole distribution of $G-M_dC_0$ when g_1 and g_2 are varying.

It can be seen from Figure 7 that the closed-loop observer has eight poles in total. λ_1~λ_8 represent all the eigenvalues of matrix G-M_dC_0. When g_1 and g_2 are both negative, we can see from Figure 7a that the system has a pole on the right side of z-plane which is far away from the unit circle. The observer is unstable in this situation. In the process of changing g_1 from negative to positive numerically, this pole can gradually approach and, finally, enter into the unit circle. It means that g_1 should be greater than zero when g_2 is negative. Figure 7b shows the locus of the poles distribution when g_1 is positive and g_2 changes from negative to positive numerically. The poles move from the inside towards the outside of the unit circle, which means the observer tends to be unstable. As a brief conclusion, the parameters g_1, g_2 directly affect the stability and performance of DOB; thus, their values must be designed carefully.

However, the order of synthesized matrix equals to eight. Therefore, it is difficult to accurately arrange all the poles to the specified positions by traditional method of tuning the coefficients of the characteristic equation. To solve this problem, this paper adopts the parameter scanning method to traverse the adjustable parameters g_1 and g_2 at a certain step within a specified range. For each step, the procedure of detecting the pole positions of observer is repeatedly carried out. The judgment of whether the stability criterion is met executes for each point (g_1, g_2) before proceeding to the next step. The scanning process will keep running until all the points in the specified range have been traversed once. The detailed scanning flow chart is shown in Figure 8. Finally, the stable region of g_1 and g_2 applicable to the specified LCL parameters listed in Table 1 is shown in Figure 9. We can deduce that g_2 should be negative and should not be too large. When g_1 increases, the optional range of g_2 also become wider.

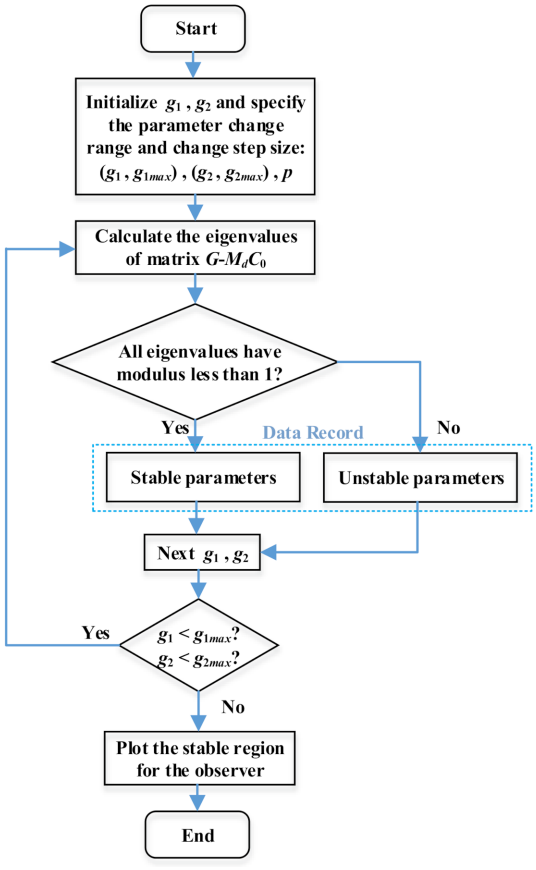


Figure 8. Flow chart for parameter scanning algorithm.

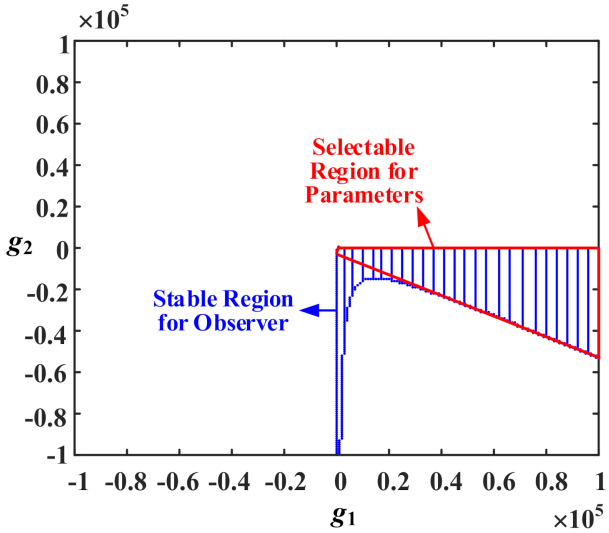
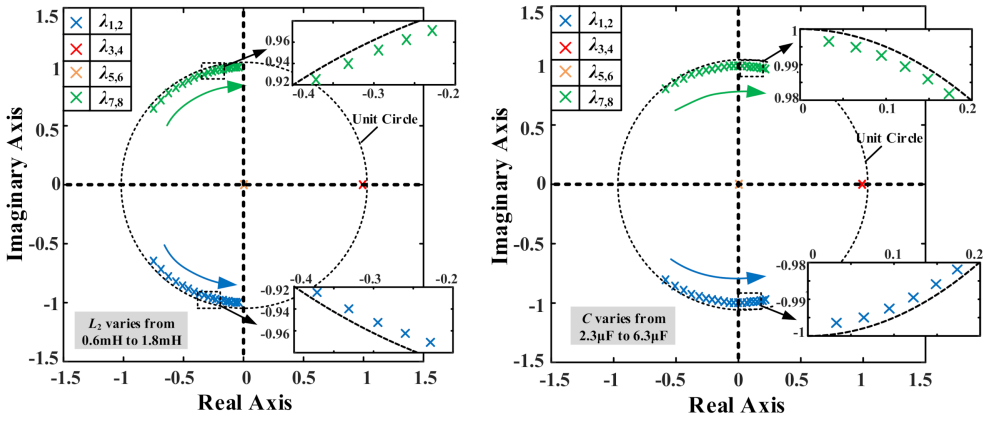


Figure 9. Stable region for parameter g_1 and g_2 obtained by parameter scan.

Although the feedback matrix can be decided through the above-mentioned parameter scanning method, some abnormal situations might challenge the stability of DOB. For example, the grid-side inductor L_2 changes under the influence of the grid impedance L_g and its accurate value is hard to be determined. Moreover, the actual parameters of filter capacitors usually fluctuate after a long-time operation. Therefore, the robustness of DOB while the parameters of LCL filter are changing should also be examined. Figure 10 shows the varying trend of the pole distribution when different main circuit parameters are substituted in order to confirm the adaptability and robustness of DOB. According to Figure 10, we can see that the changes in L_2 and C have similar effects on the pole positions of the DOB. The poles close to the origin and the real axis are not significantly affected. However, the conjugate poles in the left half plane gradually move to the right side when L_2 and C increase. The pole positions during this change all keep inside the unit circle. Therefore, the DOB maintains its ability in such circumstances. Thus, its robustness can be guaranteed.



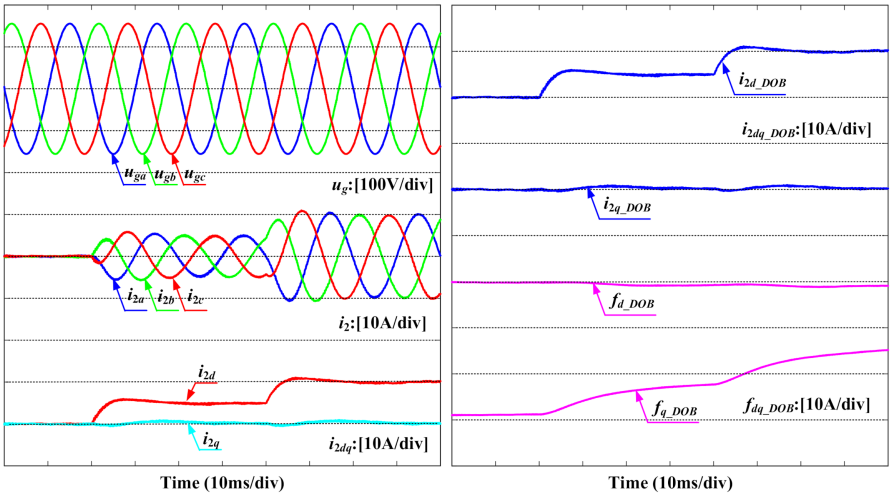
(**a**) Pole distribution when L_2 changes (**b**) Pole distribution when C changes

Figure 10. Variation trend for pole distribution of the DOB in case of parameter drift.

4. Simulation and Experimental Results

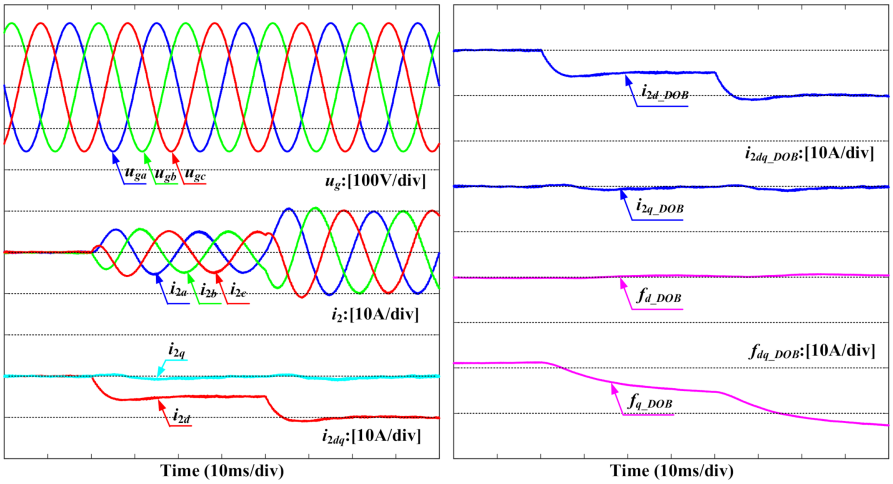
For purpose of verifying the control effect and feasibility of the algorithm presented in this paper after adding AD to the LCL filter based on DOB. The simulation model is built up in Matlab/Simulink by realizing the diagram shown in Figure 1. The system parameters are given in Table 1. The value of virtual resistor is set to 50 Ω.

To evaluate the steady state and dynamic performance of the PCS with the presented control algorithm, the start-up process of PCS for discharging operation is tested first. The reference d-axis current i_{2dref} is directly set to 5 A at 20 ms. Then, at 60 ms, i_{2dref} is set to 10 A. Meanwhile, i_{2qref} is kept as 0 A for unity power factor operation during this process. The simulation results are shown in Figure 11a. It can be seen that the grid-injected current is of good quality and can track the reference value accurately. At the same time, waveforms of disturbances estimated by the DOB are shown in Figure 11b, which include both the internal coupling items and external disturbances of the PCS. Therefore, DOB is able to estimate the unmeasurable disturbances that need to be compensated in different conditions as an enhancement for anti-interference ability of the overall system. The similar simulation results are given in Figure 12 to verify the feasibility of control method for charging condition.



(**a**) Waveforms of u_g and i_2 (**b**) Waveforms of observed i_{2dq} and f_{dq}

Figure 11. Simulation waveforms for nominal discharging operation.



(**a**) Waveforms of u_g and i_2 (**b**) Waveforms of observed i_{2dq} and f_{dq}

Figure 12. Simulation waveforms for nominal charging operation.

In order to confirm the effectiveness of the AD strategy for the LCL filter based PCS, a comparison study is carried out by invalidating the second derivative of grid-side current for a short time. The obtained simulated grid voltage and current waveforms are shown in Figure 13. AD is shut down within the time range from 30 ms to 60 ms. After AD is

disabled, it can be seen that severe current oscillation emerges immediately until AD is enabled again at 60 ms. According to the simulation results, we can deduce that the control method only relying on PI controller is not enough to suppress the resonance of LCL filter. However, this issue is effectively solved by adopting the second derivative of grid-side current feedback branch in the control loop.

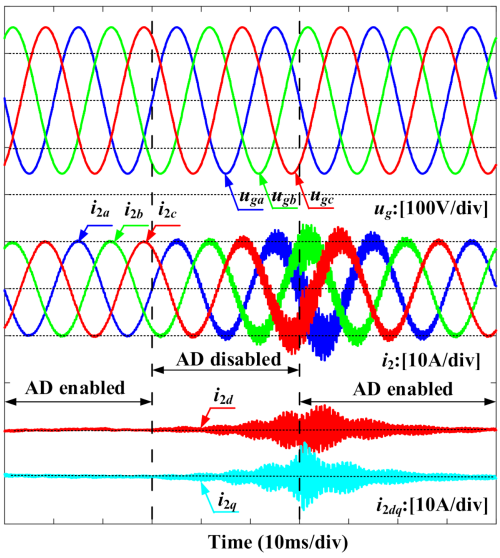
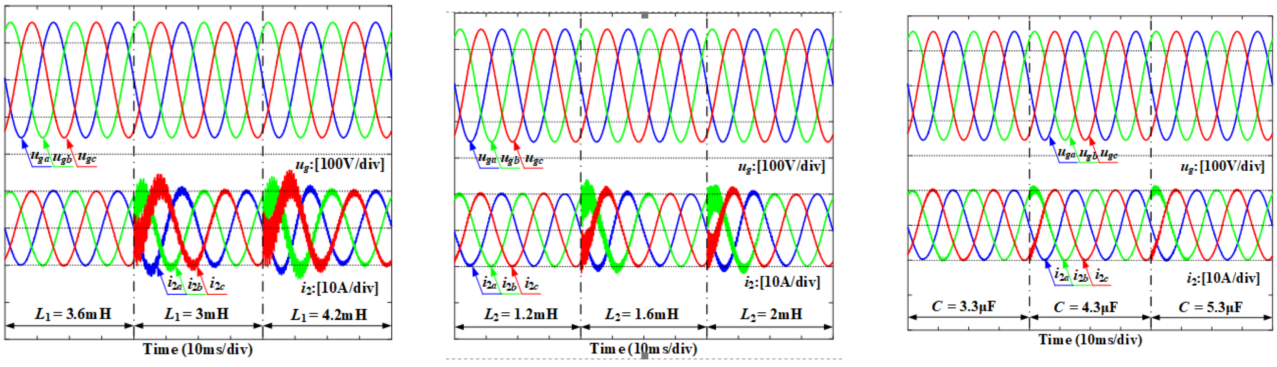


Figure 13. Comparison study for PCS with and without active damping algorithm.

In addition, the robustness of presented control method is tested too. In order to imitate the influence of main circuit parameter drift in practice, L_1, L_2 and C are deliberately set to different values with reasonable errors in the vicinity of their rated values given in Table 1, respectively. The simulation results are shown in Figure 14. Figure 14a–c depict the waveforms when parameters L_1, L_2 and C are not accurate, respectively. We can see that the negative impact of parameter drift exists but is not significant enough to cause stability problems.

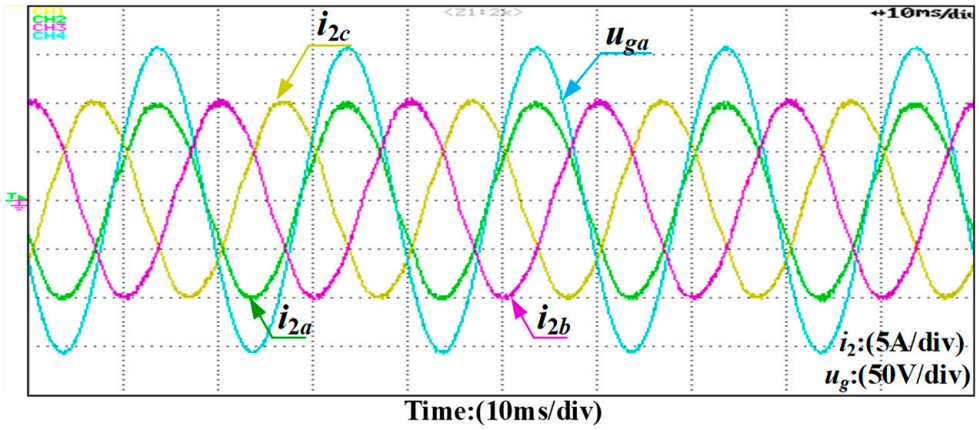


(**a**) Waveforms when L_1 changes (**b**) Waveforms when L_2 changes (**c**) Waveforms when C changes

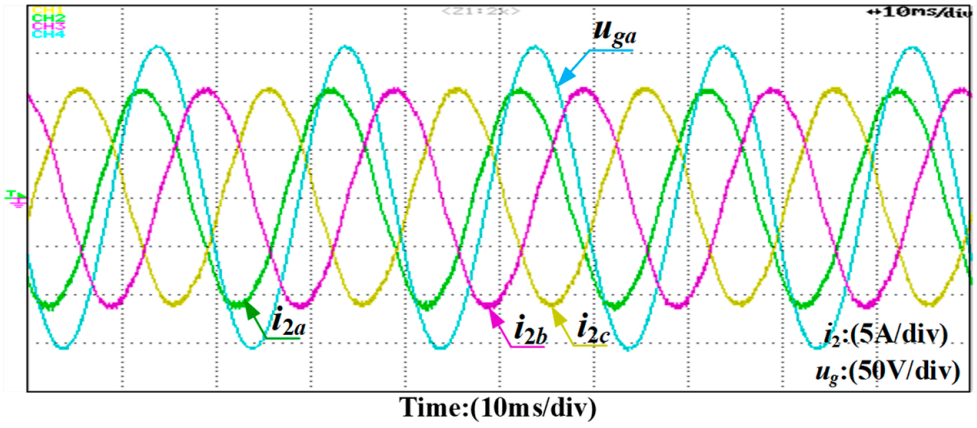
Figure 14. Simulation waveforms for PCS with LCL parameter drift.

In order to further confirm the feasibility of the presented control method, a down-scaled experimental prototype consists of dSpace and Danfoss inverter FC302 is built up. The parameters of the prototype are the same as those used in the simulation model as given in Table 1. The voltage signals are acquired by probe GWinstek GDP-025 (Suzhou, China). The current signals are acquired by probe HIOKI 3276 (Nagano, Japan). Meanwhile, the oscilloscope DL1640 manufactured by Yokogawa (Tokyo, Japan) is used to capture the waveforms.

Normal discharging operation with unity power factor is tested first. Grid voltage and current waveforms obtained from the prototype are shown in Figure 15. According to Figure 15a, we can see that unity power discharging operation is guaranteed since u_{ga} and i_{2a} always keep in phase. Grid-injected currents are all sinusoidal, which meets general power quality requirements. By setting i_{qref} to 5 A, reactive power can also be generated as shown in Figure 15b. In this situation, the current lags behind the grid voltage by approximately 25 degrees, which indicates reactive power is produced by the PCS. This function can be further used to achieve partial replacement of static Var compensator. Similar tests for charging operation are also carried out. The experimental results are shown in Figure 16. As a brief summarization, the steady state performance of PCS based on DOB can be verified.

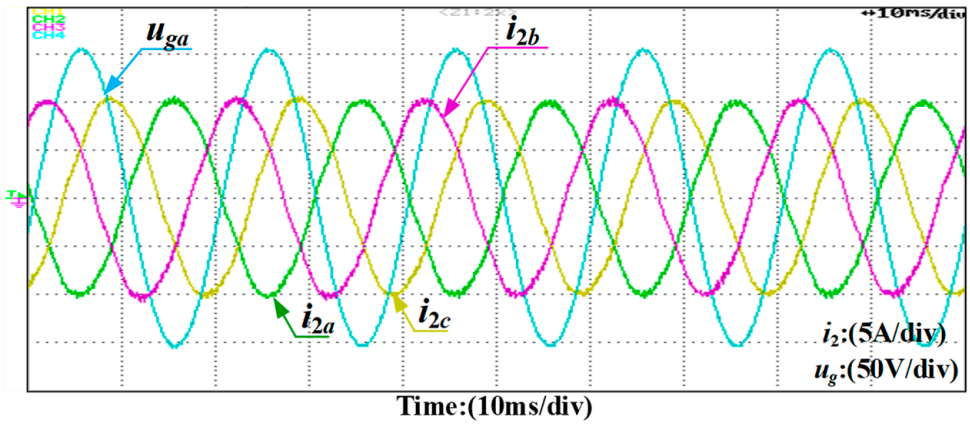


(**a**) Grid voltage and current waveforms (PF = 1.0)

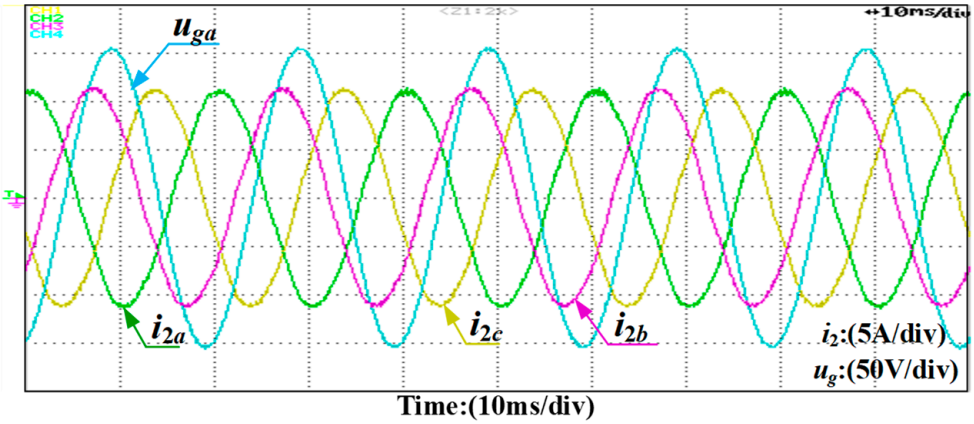


(**b**) Grid voltage and current waveforms (PF = 0.9)

Figure 15. Steady state waveforms of the PCS for discharging operation.



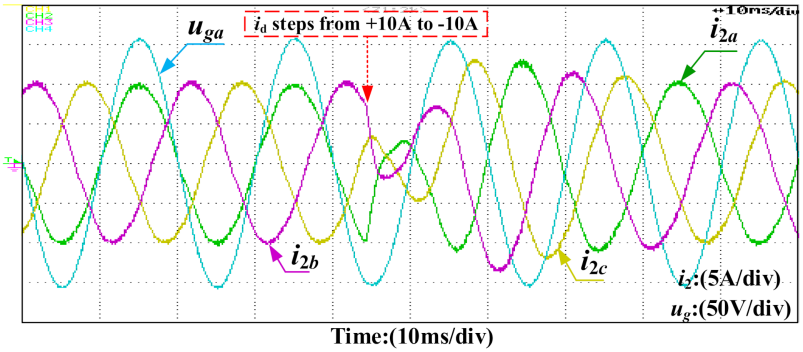
(**a**) Grid voltage and current waveforms (PF = −1.0)



(**b**) Grid voltage and current waveforms (PF = −0.9)

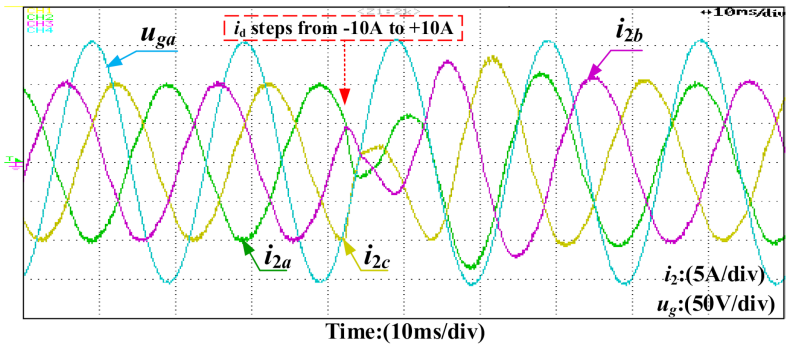
Figure 16. Steady state waveforms of the PCS for charging operation.

Furthermore, the transient response feature of PCS is tested. The experimental results obtained from the PCS prototype are illustrated in Figure 17. At first, i_{2dref} is set to 10 A. Then, it steps down to −10 A suddenly to reverse the flow direction of electric power. Based on this condition, representative test result for transition from full load discharging state to charging states is yielded as shown in Figure 17a. We can see that the full load transient process terminates within 10 ms, which meets most requirement in industrial applications. Meanwhile, the symmetrical transition from charging to discharging is also tested. Figure 17b shows the experimental results. The dynamic performance of PCS can be verified.



(**a**) Transition from full load discharging to full load charging

Figure 17. *Cont.*



(**b**) Transition from full load charging to full load discharging

Figure 17. Transient response testing waveforms of the PCS.

5. Conclusions

Damping method and disturbance rejection are both fundamental issues in a grid-tied PCS equipped with an LCL filter. In this paper, a control strategy with AD ability which involves only grid-side current as the feedback variable is studied and implemented based on DOB. The control principle is introduced and theoretical analysis is carried out in detail. Obviously, the resonance peak of filter is greatly suppressed after adopting AD controller. DOB is adopted for purpose of simultaneously estimating d^2i_{2d}/dt^2, d^2i_{2q}/dt^2 and unmeasurable disturbances. In order to guarantee the convergence for DOB, its feedback matrix is carefully designed according to the stable region calculated based on a parameter scanning method. Eigenvalue analysis verifies the robustness of DOB with parameter drift. Lastly, simulation and experimental results show that the control strategy exhibits good performance both in steady state and dynamic response.

Author Contributions: Conceptualization, N.G. and X.L.; methodology, N.G.; writing—original draft preparation, N.G. and X.L.; writing—review and editing, W.W. and F.B.; data curation, X.L.; software, X.L. and N.G.; project administration, W.W.; funding acquisition, N.G. All authors have read and agreed to the published version of the manuscript.

Funding: The research work in this paper is supported by National Natural Science Foundation of China (No. 51907119) and Shanghai Sailing Program (No. 19YF1418700).

Data Availability Statement: The data used to support the findings of this study are available from the corresponding author upon request.

Conflicts of Interest: The authors declare no conflict of interest.

References

1. Zhang, C.; Cai, X.; Rygg, A.; Molinas, M. Sequence domain SISO equivalent models of a grid-tied voltage source converter system for small-signal stability analysis. *IEEE Trans. Energy Convers.* **2018**, *33*, 741–749. [CrossRef]
2. Barba, S.L.; de la Torre, M.; Ordiales, M. New challenges for operation of systems with large renewable capacity. In Proceedings of the 2012 IEEE Power and Energy Society General Meeting, San Diego, CA, USA, 22–26 July 2012; pp. 1–6. [CrossRef]
3. Bragard, M.; Soltau, N.; Thomas, S.; de Doncker, R.W. The balance of renewable sources and user demands in grids: Power electronics for modular battery energy storage systems. *IEEE Trans. Power Electron.* **2010**, *25*, 3049–3056. [CrossRef]
4. Rocabert, J.; Capó-Misut, R.; Muñoz-Aguilar, R.S.; Candela, J.I.; Rodriguez, P. Control of energy storage system integrating electrochemical batteries and supercapacitors for grid-connected applications. *IEEE Trans. Ind. Appl.* **2019**, *55*, 1853–1862. [CrossRef]
5. Gao, N.; Chen, X.; Wu, W.; Li, X.; Blaabjerg, F. Finite control set model predictive control with model parameter correction for power conversion system in battery energy storage applications. *IEEJ Trans. Electr. Electron. Eng.* **2020**, *15*, 1109–1120. [CrossRef]
6. Chen, X.; Wu, W.; Gao, N.; Chung HS, H.; Liserre, M.; Blaabjerg, F. Finite Control Set Model Predictive Control for LCL-Filtered Grid-Tied Inverter with Minimum Sensors. *IEEE Trans. Ind. Electron.* **2020**, *67*, 9980–9990. [CrossRef]
7. Wu, W.; Liu, Y.; He, Y.; Chung, H.S.; Liserre, M.; Blaabjerg, F. Damping Methods for Resonances Caused by LCL-Filter-Based Current-Controlled Grid-Tied Power Inverters: An Overview. *IEEE Trans. Ind. Electron.* **2017**, *64*, 7402–7413. [CrossRef]

8. Beres, R.; Wang, X.; Blaabjerg, F.; Bak, C.L.; Liserre, M. Comparative evaluation of passive damping topologies for parallel grid-connected converters with LCL filters. In Proceedings of the IEEE International Power Electroniecs Conference, Hiroshima, Japan, 18–21 May 2014; pp. 3320–3337. [CrossRef]
9. Dong, M.; Ma, H.; Bai, Z. Analysis and optimizing method of transient performance for LCL-based grid-connected inverter with passive damping. In Proceedings of the 2019 10th International Conference on Power Electronics and ECCE Asia (ICPE 2019—ECCE Asia), Busan, Korea, 27–30 May 2019; pp. 2956–2961.
10. Liu, Y.; Jin, D.; Jiang, S.; Liang, W.; Peng, J.; Lai, C. An active damping control method for the LLCL filter-based SiC MOSFET grid-connected inverter in vehicle-to-grid application. *IEEE Trans. Veh. Technol.* **2019**, *68*, 3411–3423. [CrossRef]
11. Zhang, Z.; Wu, W.; Shuai, Z.; Wang, X.; Luo, A.; Chung HS, H.; Blaabjerg, F. Principle and Robust Impedance-Based Design of Grid-tied Inverter with LLCL-Filter under Wide Variation of Grid-Reactance. *IEEE Trans. Power Electron.* **2019**, *34*, 4362–4374. [CrossRef]
12. Liu, T.; Liu, J.; Liu, Z.; Liu, Z. A study of virtual resistor-based active damping alternatives for LCL resonance in grid-connected voltage source inverters. *IEEE Trans. Power Electron.* **2020**, *35*, 247–262. [CrossRef]
13. Zhou, L.; Zhou, X.; Chen, Y.; Lv, Z.; He, Z.; Wu, W.; Yang, L.; Yan, K.; Luo, A.; Guerrero, J.M. Inverter-current-feedback resonance-suppression method for LCL-type DG system to reduce resonance-frequency offset and grid-inductance effect. *IEEE Trans. Ind. Electron.* **2018**, *65*, 7036–7048. [CrossRef]
14. Zhou, X.; Zhou, L.; Chen, Y.; Shuai, Z.; Guerrero, J.M.; Luo, A.; Wu, W.; Yang, L. Robust gird-current-feedback resonance suppression method for LCL-type grid-connected inverter connected to weak grid. *IEEE J. Emerg. Sel. Top. Power Electron.* **2018**, *6*, 2126–2137. [CrossRef]
15. Yao, W.; Yang, Y.; Zhang, X.; Blaabjerg, F.; Loh, P.C. Design and analysis of robust active damping for LCL filters using digital notch filters. *IEEE Trans. Power Electron.* **2017**, *32*, 2360–2375. [CrossRef]
16. He, Y.; Wang, X.; Ruan, X.; Pan, D.; Qin, K. Hybrid active damping combining capacitor current feedback and point of common coupling voltage feedforward for LCL-type grid-connected inverter. *IEEE Trans. Power Electron.* **2021**, *36*, 2373–2383. [CrossRef]
17. Tolani, S.; Gautam, V.; Sensarma, P. Improved selective frequency active damping for voltage source inverter with output LC filter. *IEEE Trans. Ind. Appl.* **2020**, *56*, 5194–5201. [CrossRef]
18. Chen, W.H.; Yang, J.; Guo, L.; Li, S. Disturbance-observer-based control and related methods—An overview. *IEEE Trans. Ind. Electron.* **2016**, *63*, 1083–1095. [CrossRef]
19. Errouissi, R.; Al-Durra, A. Design of PI controller together with active damping for grid-tied LCL-filter systems using disturbance-observer-based control approach. *IEEE Trans. Ind. Appl.* **2018**, *54*, 3820–3831. [CrossRef]
20. Ma, W.; Guan, Y.; Zhang, B.; Wu, L. Active disturbance rejection control based single current feedback resonance damping strategy for LCL-type grid-connected inverter. *IEEE Trans. Energy Convers.* **2020**, *36*, 48–62. [CrossRef]
21. Benrabah, A.; Xu, D.; Gao, Z. Active disturbance rejection control of LCL-filtered grid-connected inverter using padé approximation. *IEEE Trans. Ind. Appl.* **2018**, *54*, 6179–6189. [CrossRef]
22. Yan, L.; Wang, F.; Dou, M.; Zhang, Z.; Kennel, R.; Rodríguez, J. Active disturbance-rejection-based speed control in model predictive control for induction machines. *IEEE Trans. Ind. Electron.* **2020**, *67*, 2574–2584. [CrossRef]
23. Khan, S.A.; Guo, Y.; Siwakoti, Y.P.; Lu, D.D.; Zhu, J. A disturbance rejection-based control strategy for five-level T-type hybrid power converters with ripple voltage estimation capability. *IEEE Trans. Ind. Electron.* **2020**, *67*, 7364–7374. [CrossRef]
24. Guan, Y.; Xie, Y.; Wang, Y.; Liang, Y.; Wang, X. An active damping strategy for input impedance of bidirectional dual active bridge DC–DC converter: Modeling, shaping, design, and experiment. *IEEE Trans. Ind. Electron.* **2021**, *68*, 1263–1274. [CrossRef]